ACADEMIC
World Academic Union

Journal of Uncertain Systems
Vol.1, No.4, pp.277-290, 2007
Online at: www.jus.org.uk

Modeling and Optimization of Film Deposition by Magnetron Sputtering

A. Axelevitch and G. Golan
Holon Institute of Technology (HIT),
P.O. Box 305, 52 Golomb St., Holon 58102, Israel
alex_a@hit.ac.il

Received 30 July 2007; Accepted 14 August 2007

Abstract

Microelectronics technological processes are most complicated and consist of many un-predicted factors on the final device parameters. Thin films deposition methods based on magnetron plasma sputtering are influenced by lots of independent active factors. These deposition methods bring along uncertainty in the precise design process of electronic components. Thus, intelligent modeling process is highly important in the design of multi-factors microelectronics system.

In this paper we present a novel approach to the deposition process of various thin films, using mathematical modeling of sputtering processes and random section method. Highly transparent and conductive indium oxide films were deposited using this mathematical modeling of magnetron sputtering method. In addition, tantalum oxide resistive thin films, with predicted properties were grown using the same method and the predicted properties were experimentally obtained.

© 2007 World Academic Press, UK. All rights reserved.

1 Introduction

Mathematical modeling of sputtering process using the random section method

Thin film vacuum deposition processes are influenced by many independent input factors (variables), including the source, the wall and the substrate temperatures, the residual, total and partial pressures, the power source strength, the vacuum chamber dimensions, the process duration, etc. Evidently, any model describing physical vacuum deposition technological process is only approximated to the ideal process. There are several different methods used to empirically study the relationships between one or more of the measured response functions, on one hand, and a number of input factors, on the other hand. One of the methods that can be used for the optimization of multi-factor systems and complex processes is the multi-simplex method [1], or the Taguchi approach [2].

The response surface methodology (RSM) is an optimization approach, which uses mathematical and statistical techniques to search for the best combination of the process variables. The response surface represents the domain of all feasible solutions for the process model [3]. The response surface approach is the best method for an empirical study of the relationships between one or more of the measured response functions such as resistivity, transparency, density, on one hand, and various input factors, on the other hand [4]. Following an empirical study, the RSM method enables the process optimization with a minimum of trial and errors. If the process model is presented as a mathematical function, one can say that the response surface is a trace of the response function (the main parameter) in the multi-factor space. Then it can be written in the form of $F = f(X_1, X_2,...X_m)$, where X_1, X_2, and X_m are the independently controlled measured input variables of the sputtering process and F is the response function.

In the narrow interval of the variation of input variables, the response function may be considered as an analytical function. The approximation process may begin as a polynomial model with linear independent coefficients [5]. Therefore, it may be expanded in a Taylor series over the chosen area in the form of:

$$f(x) = \sum_{n=0}^{\infty} \frac{f^{(n)}(x_0)}{n!}(x - x_0)^n. \tag{1}$$

By choosing the first three terms of the above expansion, a second order approximation is obtained:

$$f(x) = f(x_0) + \frac{df(x_0)}{dx}(x - x_0) + \frac{1}{2}\frac{d^2 f(x_0)}{dx^2}(x - x_0)^2. \tag{2}$$

This expression has the form of a parabolic function with linear coefficients:

$$f(x) = a + bx + cx^2. \tag{3}$$

For a multi-factor process of m levels, i.e. with m independently controlled measured input variables, the expression is transformed to a model of the following type, without the high order (in our case, third order) interaction effects:

$$\begin{aligned} F = c_0 + c_1X_1 + c_2X_2 + c_3X_3 + \ldots + c_mX_{1m} + c_{m+1}X_1X_2 + c_{m+2}X_1X_3 + \\ + \ldots + c_kX_{m-1}X_m + c_{k+1}X_1^2 + c_{k+2}X_2^2 + \ldots + c_{k+m}X_m^2 \end{aligned} \tag{4}$$

where c^i are the model coefficients, and X_i are the processing factors. A standard form for a planned series of experiments for evaluating the normalized process factors is shown in Table 1. The factors are normalized using the following equation:

$$Xi^* = 2(Xi - X0)/\Delta X, \tag{5}$$

where X_0 is the midpoint of the variable range, and ΔX is the variation range.

For instance, Figure 1 illustrates an example of a bi-factor space. The coordinate axes X and Y represent two active technological factors (examples). Axis Z, in its turn, represents the response function (example), which can also be named “an object function”. The response function draws a surface in the multi-factor space, called the response surface. The response function can be studied with the help of the RSM method and then optimized. Optimization of this mathematical model is obtained by moving in the direction of the function’s gradient slope. The function optimum (extreme) is achieved under the following conditions:

$$\nabla f\,(X_1X_2\ldots X_m) = 0, \tag{6}$$

and

$$\partial^2 f\,(X_1, X_2, \ldots X_m) < 0 \text{ (for the maximum)}. \tag{7}$$

Obviously, in order to create a complete multi-factor space from the m variable system, a minimum of 2m separate experiments are required; the constants can then be calculated from the 2m resulting equations. In addition, a few more experiments in the system center ($X_i^* = 0$) are required in order to estimate the error of the calculated result. However, from a practical point of view, there is no need to run all of these

experiments. It is possible to complete only a few experiments and then deduce the missing coefficients using the mathematical procedure known as “estimation on partial sections in multi-factor space”[6]. According to this procedure, each one of the experiments is actually a partial section of the chosen multi-factor space. Consequently, the coefficients of the approximation model must be related for all partial sections. Thus the missing coefficients can be calculated by varying one parameter in the following quadratic model:

$$\begin{cases} c_1 + c_2 x + c_3 x^2 = F_k(x = x_k) \\ c_1 + c_2 x + c_3 x^2 = F_{k+n}(x = x_{k+n}) \\ c_1 + c_2 x + c_3 x^2 = F_{k+m}(x = x_{k+m}) \end{cases} \tag{8}$$

where c_i is the missing coefficient, x – the process parameter (X_1,X_2,..X_N), and m, n are indices. The rest of the missing coefficients describing the required model are then obtained by solving the coefficient matrix with the Kramer method. A virtual example of a multi-factor space experiment and a random partial section of it are shown in Figure 2. Here, each partial section of the multi-factor space (sphere) represents a circle situated in the space accordingly to the experiment.

In the case of a large deviation between the measured data and the model, the approximation order, i.e. the order of approximation equation, should be increased.

2 Deposition of In_2O_3 Conductive Transparent Coatings by DC Sputtering

2.1 Preamble

Transparent conductive coatings with high electrical conductivity and maximum optical transparency have attracted much attention in recent years. These coatings have many practical applications, such as transparent electrodes in microelectronics, optoelectronic devices and photovoltaic systems.

Indium oxide thin films possess the electronic properties of n-type semiconductors with a band gap in the range of 3.5 to 4 eV. Oxygen vacancies in the films provide free electrons by acting as doubly charged donors. Since the indium oxide films generally suffer from oxygen deficiency, the electron gas in the conduction band is degenerate [7]. These transparent films are often alloyed with tin oxide (5 to 10 %); these films are known as indium tin oxide (ITO). ITO films have a higher free charge concentration, which increases the electrical conductivity [8]. Films without tin admixture have higher resistivity and lower transparency than ITO [9]. The tin is commonly believed to provide free electrons by substituting for the indium atoms and acting as a singly charged donor at the indium site.

Most of the unalloyed indium oxide films were prepared by various evaporation methods. These methods had one common characteristic: admitting of oxygen in the vacuum chamber (reactive evaporation) [10]. The influence of oxygen on the partial pressure of the structure of the reactively deposited indium oxide films has been described in ref. [11]. In ref. [12], the influence of the substrate temperature, deposition rate, base and background pressures, and alloy constituents concentration were studied. However, the films with maximum transparency and minimum resistivity have been prepared by sputtering methods [13].

2.2 Experimental Procedure

The experiments were carried out on a laboratory magnetron sputtering vacuum station equipped with a diffusion pump. The residual pressure prior to the deposition process was less than 4×10^{-5} Torr and sputtering was done in a pure argon atmosphere (99.99 %). The substrate temperature was varied during the deposition process. The indium oxide films were deposited on a borosilicate glass plate 0.13-0.17 mm thick and on an optical glass 1 mm thick. The sputtering target was in a shape of a round disk, 50 mm in

diameter and 3 mm thick, made of pure indium oxide (99.999%). The substrate-to-target distance was taken as 5 cm.

We evaluated the optical and electrical properties of the resultant In_2O_3 films. The optical transparency of the films and absorption for $250 < \lambda < 880$ nm wavelength, was determined on a Uvicon 941 Plus spectrophotometer. A computerized metallurgical microscope with magnification ×80 to ×1600 was used for the micro-topography evaluation. The micro-hardness of the resulting films was measured using a PMT-3 tester. The indentation period was 15 seconds; 5 to 10 indentations were taken for each specimen. Before deposition, the substrates were cleaned with alcohol in the ultrasound heater for 5 min.

The most significant properties of In_2O_3 films are their transparency and resistivity. These properties were defined as the response functions. The active technological factors for the sputtering model were taken as follows: P_{Ar} - argon pressure (1.5 ÷ 2 Torr), Vt - DC voltage to the target (500 ÷ 750 V), T_s - substrate temperature (150 ÷ 250° C), and t - deposition duration (20 ÷ 40 min), and the model was written in the form: F = *f*(P,V,T,t). A complete factor experiment of the order of 2^4 yields the following regression equation with 15 coefficients:

$$\begin{aligned} \mathrm{F} &= a_1 + a_2 P_{Ar} + a_3 V_t + a_4 T_s + a_5 t + a_6 P_{Ar} V_t + a_7 P_{Ar} T_s + a_8 P_{Ar} t + a_9 V_t T_s + \\ &+ a_{10} V_t t + a_{11} T_s t + a_{12} P_{Ar}{}^2 + a_{13} V_t^2 + a_{14} T_s{}^2 + a_{15} t^2 . \end{aligned} \tag{9}$$

2.3 Practical Model Implementation

It is obvious that in order to create a complete 15-constant "factor space" from a 4-variables system, 15 separate experiments should be carried out. These constants will be then calculated from the 15 obtained equations. In addition, it is necessary to perform a few more experiments in the system center in order to obtain an estimation of the relative experiment error. One should always bear in mind that only the first few resultant coefficients were experimentally obtained, while the rest of the coefficients were derived mathematically from following matrix (i is an index):

$$\left(1\ \mathrm{P_i}\ \ \mathrm{V_i}\ \ \mathrm{T_i}\ \ \mathrm{t_i}\ \ \mathrm{P_iV_i}\ \ \mathrm{P_iT_i}\ \ \mathrm{P_it_i}\ \ \mathrm{V_iT_i}\ \ \mathrm{V_it_i}\ \ \mathrm{T_it_i}\ \ \mathrm{P_i^2}\ \ \mathrm{V_i^2}\ \ \mathrm{T_i^2}\ \ \mathrm{t_i^2}\right) = \left(\mathrm{a_i}\right)\cdot\left(\mathrm{F_i}\right). \tag{10}$$

At this point the optimization model of equation (6) can be implemented.Thus, the optimization problem is transformed to the following gradient relation:

$$\partial\, \mathrm{F}(\mathrm{P_*}, \mathrm{V_*}, \mathrm{T_*}, \mathrm{t_*}) = \nabla \mathrm{F}(\mathrm{P_{Ar}}, \mathrm{V_t}, \mathrm{T_s}, \mathrm{t}) \cdot \begin{pmatrix} \partial\, \mathrm{P_{Ar}} \\ \partial\, \mathrm{V_t} \\ \partial\, \mathrm{T_s} \\ \partial\ \mathrm{t} \end{pmatrix} = 0\,, \tag{11}$$

where $F(P_*,V_*,T_*,t_*)$ is the required extreme. Analysis of this relation yields 16 possible combinations (2^4) between the four variables. Similarly, analysis of the second derivative yields the type of extreme: a maximum for the transparency and a minimum for the resistivity.

2.4 Experimental Results

The film morphology shows a very homogeneous smooth surface without hillocks usually observed on evaporated films. A SEM microstructure analysis of the films indicated good homogeneity with grain dimensions smaller than the microscope resolution.

The diagram in Figure 3 shows the dependence of the partial oxygen pressure and the substrate temperature on the film phase composition [11]. This diagram is drawn up for the films obtained by thermal evaporation of pure indium in oxygen atmosphere. The diagram shows the variation range of the technological factors that enable the indium – indium oxide mixture: the substrate temperature T = 60 to 250 °C and the partial oxygen pressure Po ≤ 1.5×10^{-4} Torr.

In our case, there are two important distinctions: the sputtered particles are partially excited atoms of In and O with energies in tens times higher than those of evaporated particles [14]. Besides, the oxygen partial pressure was lower than 1×10^{-5} Torr (residual gas only). Therefore we can assume that our films are mixtures of different oxides of indium ($InO + In_2O + In_2O_3$), which have different temperatures of formation and heat capacity [13]. Under the conditions of free oxygen atom deficiency, complete oxidation of all sputtered particles is impossible. Fig. 4 shows a typical transparency characteristic near the absorption edge.

The band gap of the grown films increases with further In oxidation. As shown in Figure 4, the maximum transparency of the coating reaches up to 98% that yields an antireflection effect. The energy band gap of the obtained In_2O_3 films was found by plotting the relation:

$$\alpha(h\nu) = A(h\nu - E_g)^{1/2} \tag{12}$$

where E_g is the band gap, for direct impurity transitions [10]. The least square method was used for extrapolation and finding the intersection point of the function (12) and the abscissa axis, i.e. the band gap [15]. The maximum band gap value was found to be 4.08 eV for the film with maximal adhesion.

The electrical properties of the obtained films were stable enough. The active technological factors affect the electrical, mechanical and optical properties of the deposited films during deposition. Figures 5, and 6 illustrate this influence. Figure 5 shows the influence of the type of substrate and of the growth rate on the resistivity of the deposited films. Figure 6 presents the influence of the growth rate on the micro-hardness and transparency, on the wavelength of 550 nm.

Table 2 summarizes the experimental data. Each row represents a trial and is a random section of the multi-factor space. Based on these results, the coefficients were calculated for best transparency and resistivity, using the quadratic model. A regression equation using obtained coefficients was built. In this calculation, the second order interference effects should be considered as well. The required expression is derived in the following form:

$$F = 88.96 - 0.93P_{Ar} + 0.13V_t - 1.5T_s + 0.37t + 0.005P_{Ar}V_t + 0.005P_{Ar}T_s + 0.006P_{Ar}t + 0.006V_tT_s + \\ + 0.005V_tt + 0.005T_st + 0.38P_{Ar}^2 + 0.006V_t^2 + 0.006T_s^2 + 0.005t^2 . \tag{13}$$

Calculations of the optimal deposition parameters were done using the “steep rise” method (11). The optimization was done for two parameters: transparency at λ = 550 nm and sheet resistance.

The absorption edge of the film after optimization corresponds to the transparency of the In_2O_3 film at the energy gap of ~ 3.88 eV. Variation of the process parameters enabled us to control the shift in the absorption edge value, the value of maximum transparency and the transparency curve shape. The model error for (13) was evaluated at the point (-1,-1,-1,1), and the relative error in the chosen space of active parameters was:

$$\delta = \frac{|\Delta|}{F_{(-1,-1,-1,1)}}100\% = \frac{93.47 - 91.63}{91.63}100\% = 2\% . \tag{14}$$

This small error proves that the proposed model is adequate and can be used to set magnetron deposition parameters. The designed model coefficients (regression coefficients) can be presented as coefficients of

Taylor expansion around the points of interest. This approximation method is very convenient, since the accuracy of the solution system can be enhanced by increasing the degree of the original Taylor series.

The main disadvantage of this model lies in the need of quadratic approximation for multi-factor processes, due to inaccuracy of the linear approximation. It should be noted that even the quadratic approximation does not precisely represent the situation since the real function may be too complicated. The best In_2O_3 films have transparency of 90.7 % at λ = 550 nm and resistivity of 0.043 Ω·cm for a thickness of ~252 nm.

3 Deposition of Ta Resistive Coatings with Specified Conductivity

3.1 Preamble

Tantalum films were widely used as resistive coatings since the early sixties. These films feature a negative temperature resistance coefficient (NTC), superconductivity at low temperatures (4 K for the bulk tantalum and 40-50 K for the tantalum oxide thin films), and a wide range of resistivity at low temperatures (10 to 1000 μΩ·cm at 0 to 30 % oxygen content) [16]. During the nineties, tantalum films were successfully applied in microelectronic applications owing to their attractive physical properties such as high dielectric constant (~20-40), transparency in the spectrum range of 0.4 μm to 8 μm, high durability, corrosion resistance, and excellent mechanical protection to the layers underneath [17].

All of these advantages of tantalum oxide thin films make them usable for a wide variety of electrical and mechanical applications. Tantalum oxide films were applied in capacitors and in MOS transistors in dynamic random access memories (DRAM) [18], as photosensitive materials in Bragg's gratings for optical waveguides [19], and as a protection layer in photosensitive device systems. Ta_2O_5 films were applied as membranes in biomedical systems [20] due to their biological compatibility with blood and other biological matters.

Deposition techniques for tantalum oxide films and their conductivity mechanisms were studied in several reports [21]. In these and some other researches the tantalum oxide films were presented as a mixture of metallic Ta and insulating Ta_2O_5. One of the models [22] presents the electrical conductivity of the Ta + Ta_2O_5 system as a function of the fractional volume of tantalum particles in the tantalum oxide matrix. However, the experiments showed the conductivity to decrease much faster than predicted by the model. Then the authors suggested an activation model of the process, i.e. $\sigma \propto \exp(-\Delta E/T)$, where ΔE is the activation energy. Therefore, the non-linearity was suggested to be the result of a combination of metallic and tunneling conductivity. Another proposed explanation implied the excess tantalum to form donor levels along the band gap of Ta_2O_5.

Tantalum is a refractory (high-melting temperature) metal. Its vapor pressure reaches 10^{-2} Torr at its melting point, 3000 °C. Tantalum thin films are usually formed by sputtering methods [23] or by electron–beam evaporation [19]. Resistive tantalum films are usually solid solutions of (Ta + Ta_2O_5) or (Ta + Ta_2N). The type of deposition usually used for these films is reactive sputtering.

In our work we tried to use the RSM ideas for mathematical modeling of the magnetron sputtering. Here, we used such modeling for the deposition of thin film resistors consisting of tantalum and its oxides. A feasibility of depositing tantalum films with the specified resistance values controlled by variation of the technological parameters was successfully proved.

3.2 Experimental Procedure

Experiments were done using the same laboratory magnetron sputtering vacuum station [24]. Glass microscope slides of 25*75 mm^2 were used as substrates in all experimental trials. Residual gas was used as an active oxidizing reactive agent. The following five independent technological parameters were varied in the deposition experiments:

- V, sputtering voltage: 1.5 to 2.5 kV;
- PAr, argon pressure: 70 to 300 mTorr;
- Pres, residual air pressure: $2.5*10^{-5}$ to $7.5*10^{-5}$ Torr;
- T_s, the substrate temperature: 200 °C;
- t, deposition duration: 1.5 to 2.5 hours.

A standard four-point probe method was used for the sheet resistance measurement. Each sample was measured in several points, and the averaged results were used for further estimations. The surface structure of the obtained films was studied on a computerized metallurgical microscope. Film thickness was measured on the homemade computerized micro-interferometer [25].

3.3 Practical Model Implementation

A magnetron sputtering process was described in the form of an equation $F = f(x_1,x_2,..x_i,..x_n)$, where x_i are the process factors. The process analysis enabled us to use only several factors, while taking other factors as insignificant. For the first level approximation, we chose the following equation:

$$F = f\,(P_{res}, P_{Ar}, V, T_s, t), \qquad (15)$$

where P_{res} is the residual pressure in the vacuum chamber, P_{Ar} – the working argon pressure, V – the sputtering voltage, Ts – the substrate temperature, and t – the deposition duration.

In order to provide complete evaporation of the air and water molecules from the substrate, we chose Ts = 200 °C for all the experimental trials. This temperature was not essential for the metal film growth [26], but enabled better adhesion to the substrate. The deposition duration was two hours. With sufficiently thick tantalum layers, we can neglect the initial stage of film growth. The long deposition duration also allows us to neglect the influence of the residual pressure, due to a relatively high pressure of argon gas in the course of the 2-hour process.

Therefore, for such a deposition process the following approximation model can be applied:

$$\sigma = f(P_{Ar}, V). \qquad (16)$$

Here the conductivity σ represents a response function of two variables. Suppose that the response function is analytical, so that it can be expanded in a Taylor series [27]. The first three terms represent a classical second-degree equation. Therefore, the resulting equation can be written as:

$$\sigma = a_1 + a_2P_{Ar} + a_3V + a_4P_{Ar}V + a_5P_{Ar}^2 + a_6V^2. \qquad (17)$$

3.4 Experimental Results

Table 3 represents the tantalum Film conductivity as a function of two variables: the argon pressure and the sputtering voltage. As seen, the factors were varied in a random way. Therefore, each experimental trial represents a partial section of the chosen multi-factor space [27], and the required model can be built with the missing coefficients.

The tantalum films shown in Figure 7 were deposited with various argon pressures. It can be observed that the surface roughness of the obtained films increases with higher pressures. The surface roughness usually reflects the presence of spot defects or second phase inclusions. It is reasonable to assume that these defects are crystal inclusions of the tantalum oxide film in the metal tantalum matrix. Therefore, when the number of these inclusions (spot defects) exceeds the defined threshold level, the activation type of conductivity become prevailing over the metallic type.

This reasoning originates from figure 8, which represents in a graphical form the dependence of conductivity on the working pressure, for various sputtering voltages. It is easily observed that the graphs $\sigma = f(P_{Ar})$ are similar to each other for various sputtering voltages. As shown in these graphs, conductivity decreases with the increase in the working pressure. The area on the graph with a sharp bending, in which the tantalum electrical properties drastically change, is clearly observed. At this threshold level, marking the change in the tantalum films composition structure, the activation type of conductivity becomes prevailing over the metallic type.

As seen from Table 3 and Figure 8, the experimental data contain missing points. In other words, a number of experimental trials were insufficient for the table 3 filling. In our case, the missing points and the model coefficients can be calculated using a polynomial interpolation method [28]. As in the Newton Divided-Difference Interpolation Polynomial method, the following formula similar to the Taylor's expansion can be applied:

$$\sigma(P_{Ar}) = f(x) = P_n(x) + R_n(x), \tag{18}$$

where f(x) is the response function, $P_n(x)$ is the interpolation polynomial and $R_n(x)$ is the approximation error. $P_n(x)$ equals f(x) in the specified points: $x_0, x_1, \ldots x_n$, therefore, the values of $x = P_{Ar}$ are the interpolation centers.

The 3rd degree interpolation polynomial, in our case, can be written in the form of:

$$P_n(x) = f[x_0] + (x - x_0)f[x_1,x_0] + (x - x_0)(x - x_1)f[x_2,x_1,x_0] + + (x - x_0)(x - x_1)(x - x_2)f[x_3,x_2,x_1,x_0], \tag{19}$$

where

$$f(x_n, x_{n-1}, \ldots, x_0) = \frac{f(x_n)}{(x_n - x_{n-1})\cdots(x_n - x_0)} + \frac{f(x_{n-1})}{(x_n - x_{n-1})\cdots(x_n - x_0)} + \\ + \ldots + \frac{f(x_0)}{(x_n - x_{n-1})\cdots(x_n - x_0)} = \sum_{i=0}^{n} \frac{f(x_i)}{\prod_{\substack{j=0 \\ j\neq i}}^{n}(x_i - x_j)}. \tag{20}$$

This model can be re-written in the Lagrange form, for higher levels of interpolation. Thus, the coefficients of the process model can be calculated from the following formula:

$$P_n(x) = \sum_{i=0}^{n} \frac{f(x_i)\prod_{\substack{j=0 \\ j\neq i}}^{n}(x - x_j)}{\prod_{\substack{j=0 \\ j\neq i}}^{n}(x_i - x_j)}. \tag{21}$$

Estimation of the required coefficients gives the following specific model:

$$P_3(x) = -2.55*10^{-3}x^3 + 1.39x^2 - 250.81x + 14216. \tag{22}$$

Figure 9 represents this $P_3(x) \approx \sigma(P_{Ar})$ for the sputtering voltage of V = 1.5 kV. As shown, the estimated point fits the experimental graph without disfiguring it. Generalizing the interpolation model in 3-D [29] using the Lagrange form yields the response surface shown in Figure 10.

This graph enables the deposition of tantalum films with pre-defined conductivity in the chosen areas of the technological factor variations. Thus, we have demonstrated the possibility to successfully apply the proposed engineering method to experiment planning and development of various deposition technologies.

Conclusions

As shown, the RSM method enables us generate a model of a multi-factor thin film deposition process as well as its optimization. Moreover, this method enables us to design predicting models of technological processes in microelectronics, in conditions of uncertainty in the background information.

From a practical point of view, the described method is of a great interest. Using this method, good results may be obtained without performing a large number of trial and error experiments in order to develop a specific coating technology. Furthermore, it is no longer necessary to have complete knowledge of all the required process parameters.

References

[1] MultiSimplex, Design of experiments optimization strategies, http://www.multisimplex.com/strategy1.htm
[2] Resit Unal, Edwin B. Dean, Taguchi approach to design optimization for quality and cost: an overview, http://techreport.larc.nasa.gov/ltrs/91/conf-13-ispa-unal%2bdean.refer.html
[3] Box, G., W. Hunter and J. Hunter, *Statistics for Experimenters: An Introduction to Design, Data Analysis, and Model Building*, John-Wiley, N.Y.,1978.
[4] Voznesensky, V. A., *Experiment Planning Statistical Methods for Technical and Economical Investigations*, Statistics, Moscow, (Russian), 1974.
[5] Moshinsky, L., *Epoxy Rresins and Hardeners*, Arcady-Press, Tel-Aviv, (Russian), 1995.
[6] Golan, G., A. Axelevitch and E. Rabinovitch,, A linear model application for the design of transparent conductive In_2O_3 coatings, *Microelectronics Journal*, vol.29, pp.689 - 694, 1998.
[7] Bellingham, J. R., W. A. Phyllips and C. J. Adkins, Electrical and optical properties of amorphous indium oxide, *J. Phys.: Condens. Matter*, vol. 2, pp.6207 – 6221, 1990.
[8] Shigesato, Y., D. C. Paine, A microstructural study of low resistivity tin indium oxide prepared by D.C. magnetron sputtering, *Thin Solid Films*, vol. 238, pp.44 - 50, 1994.
[9] Murkherjee, A., The deposition of transparent conductive oxide thin films onto large sheets of glass, acrylic and polycarbonate, *Vacuum*, vol.39, pp.537 - 540, 1989.
[10] Naseem, S., M. Iqba and K. Hussain, Optoelectrical and structural properties of evaporated indium oxide thin films, *Solar Energy materials and Solar Cells*, vol.31, pp.155 - 162, 1993.
[11] Muranaka, S., H. Hirooka and Y. Bando, Influence of oxygen pressure on the structure of reactively deposited indium oxide films, *J. Mater. Chem.*, vol.3, no.3, pp.237 - 240, 1993.
[12] Mirzapour, S., S. M. Rozati, et al., Dependence of structural and electrical properties of undoped spray-deposited indium oxide thin films on deposition temperature, *Materials Letters*, vol.13, pp.275 - 278, 1992.
[13] Joshi, R. N., V. P. Singh and J. C. McClure, Characteristics of indium tin oxide films deposited by r.f. magnetron sputtering, *Thin Solid Films*, vol.257, pp.32 - 35, 1995.
[14] Christou, C., Z. H. Barber, Ionization of sputtered material in a planar magnetron discharge, *J. Vac. Sci. Technol.* A, vol.18, no.6, pp.2897 – 2907, 2000.
[15] Kasiviswanathan, S. and G. Rangarajan, Direct current magnetron sputtered In_2O_3 films as tunnel barriers, *J. Appl. Phys.*, vol.75, no.5, pp.2572 - 2577, 1994.
[16] Westwood, W. D., N. Waterhouse and P. S. Wilcox, *Tantalum Thin Films*, Academic Press, New York, 1975.
[17] Chen, K., M. Nielsen, S. Soss, et al., Study of tantalum oxide thin film capacitors on metallized polymer sheets for advanced packaging applications, *IEEE Transactions on Components, Packaging, and Manufacturing Technology Part B: Advanced Packaging*, vol.20, no.2, pp.117, 1997.
[18] Takaishi, Y., Process of fabricating dynamic random access memory device having storage capacitor low in contact resistance and small in leakage current through tantalum oxide film, *United States Patent 5*,726,083, March 10, 1998.
[19] Tantalum oxide, Ta_2O_5 for optical coating, http://www.cerac.com/pubs/proddata/ta205.htm
[20] Poghossian, A. S., The mechanism of blood-compatibility of some materials used in biomedical sensors, *Proceedings of the East Asia Conference on Chemical Sensors*, October 12-13, Supplement B, 1993.

[21] Mukaida, M., Y. Imai, et al., Electrical property of tantalum oxide films prepared by krF excimer laser chemical vapor deposition, *Tran. Mat. Res. Japan*, vol. 14A, pp.767-770, 1994.
[22] Gerstenberg, D. , C. J. Calbick, J. Appl. Phys., 35, 402, 1964.
[23] Resistor technology assessed at microwave frequencies, http://www.kditriangle.com/pdfiles/APPNOTE5.pdf
[24] Golan, G., A. Axelevitch, Ring etching zones on magnetron sputtering targets, *Thin Solid Films*, vol.300, pp.72 - 77, 1997.
[25] Axelevitch, A., R. Margolin, E. Rabinovitch and G. Golan, Sputtered ta oxide films as precision resistors, AGIL-2000, *3rd Conference of the Israeli Materials Society*, Jerusalem, Israel, 8-9 November 2000.
[26] Golan, G., A. Axelevitch, Novel sputtering method for Pd-Al_2O_3 UV transparent conductive coatings, *Microelectronics Journal*, vol.31, no.6, pp.469-473, 2000.
[27] Golan, G., A. Axelevitch and E. Rabinovitch, General technological modeling method for the design of transparent conductive In_2O_3 electrodes, *J. Vac. Sci. Technol*., A, vol.16, no.4, pp.2614-2618, 1998.
[28] Cernahan, B., H. A. Luther and J. O. Wilkes, *Applied Numerical Methods*, John Wiley & Sons, N.Y., 1969
[29] Demidovich, B. P., I. A. Maron, *Calculus Mathematics Fundamentals*, (in Russian), Science, Moscow, 1970.

N	**X_1^***	**X_2^***	**X_3^***	**...**	**X_N^***	**F**
1	**+1**	**+1**	**+1**	**...**	**+1**	
2	**+1**	**+1**	**+1**	**...**	**-1**	
...	**...**	**...**	**...**	**...**	**...**	
2^m	**-1**	**-1**	**-1**	**...**	**-1**	

Table 1. Standard form for model coefficient estimation.

V_t, V	V*	P_{Ar}, Torr Torr	P*	T_s, °C	T*	t, min	t*	R□, Ω/sq	F, % %(550)
400	-1.8	2	1	20	-3.6	30	0	463714.2	90.7
700	0.6	2	1	150	-1	30	0	5142.007	86.02
750	1	1.8	0.32	250	1	30	0	5176.905	88.97
750	1	1.6	-0.32	250	1	20	-	15391.73	90.9
600	-0.2	1.9	0.84	150	-1	40	1	10656.96	91.9
500	-1	1.5	-1	150	-1	40	1	4706.079	93.47

Table 2. Illustration of random partial sections of the multi-parameter space.

V \ P_{Ar}	70	90	110	130	300
1.5	2244.67		530.79	392.7	0.01
2.0		1233.65	520.83		0.01
2.3					2.39
2.5	1075.27	645.99			331.56

Table 3. Tantalum conductivity as function of two variables.

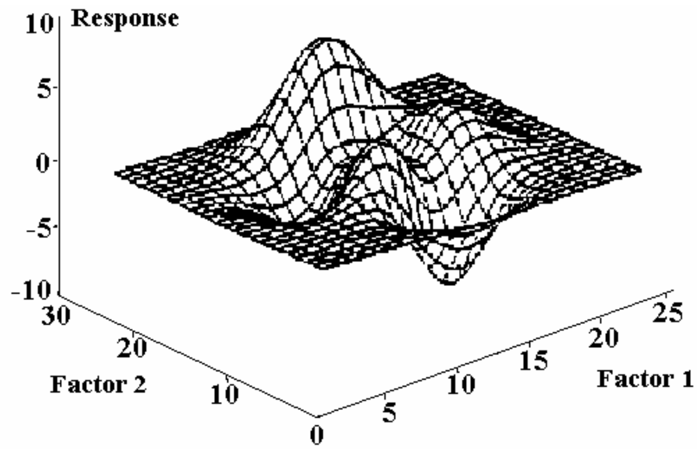

Figure 1. Example of bi-parameter experiment space.

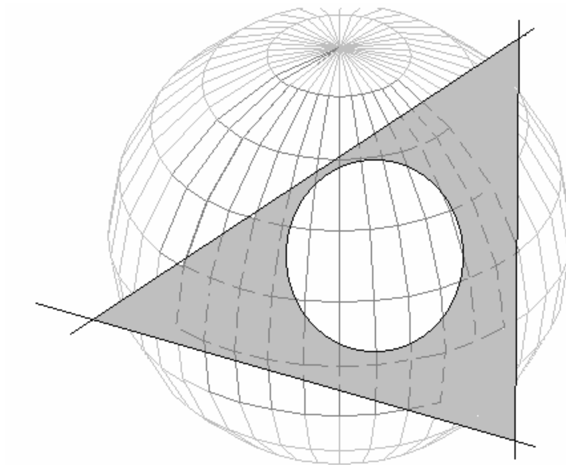

Figure 2. Illustration of random partial sections of the multi-parameter space.

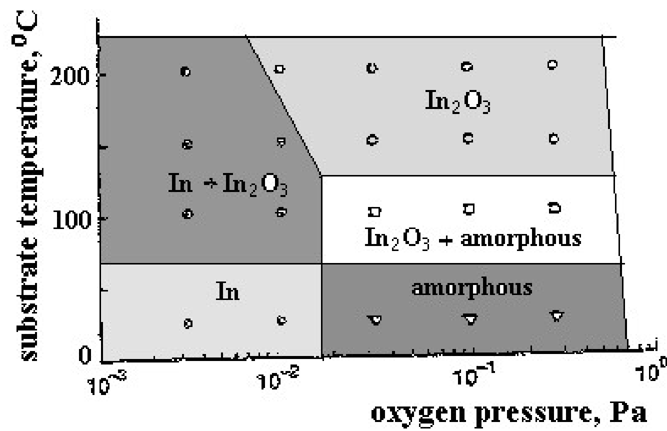

Figure 3. Evaporated ITO film composition diagram.

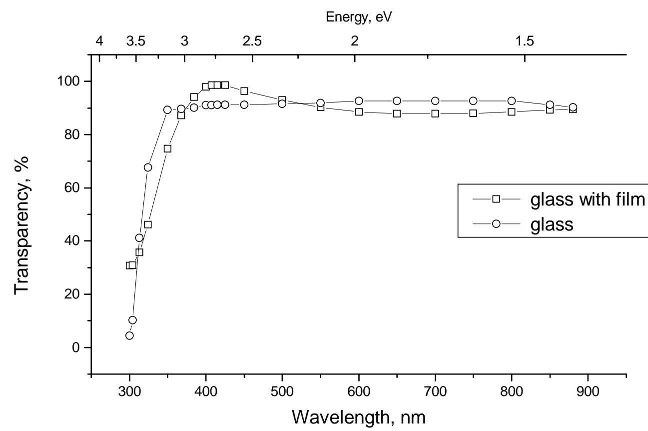

Figure 4. A typical transparency characteristic of In_2O_3 on the borosilicate glass.

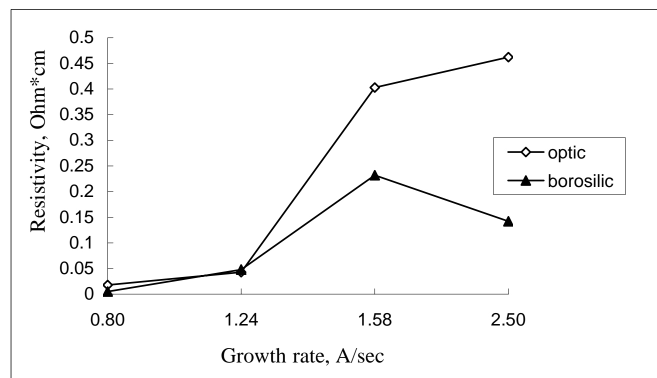

Figure 5. Resistivity of In_2O_3 film for different types of substrates.

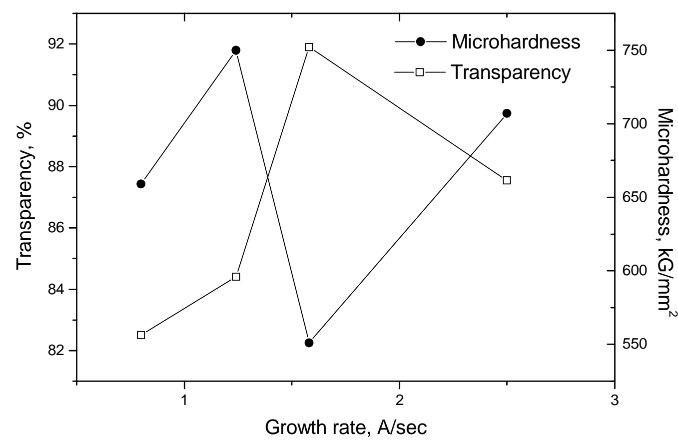

Figure 6. Influence of growth rate on In_2O_3 film properties.

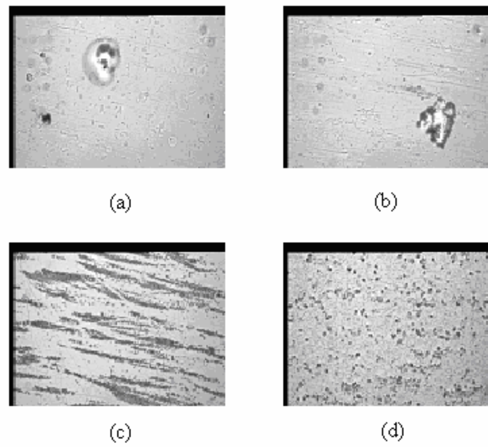

Figure 7. Tantalum thin films prepared with various argon pressure:
a –90 mTorr, b – 110 mTorr, c – 130 mTorr, d – 300 mTorr.

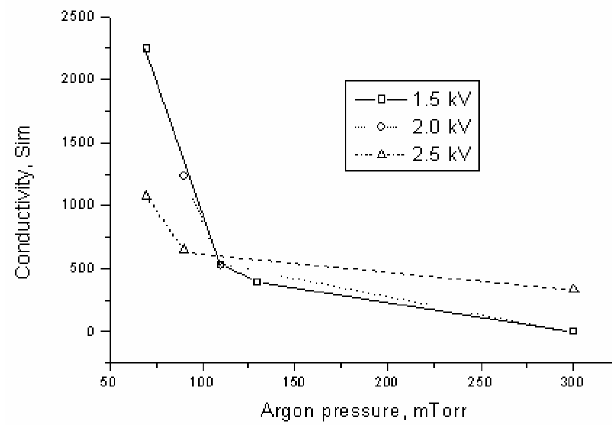

Figure 8. Conductivity of tantalum films as a function of two variables:
argon pressure and sputtering voltage.

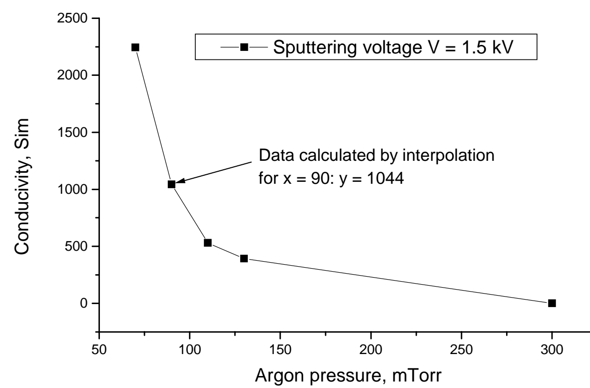

Figure 9. Tantalum film conductivity, calculated value.

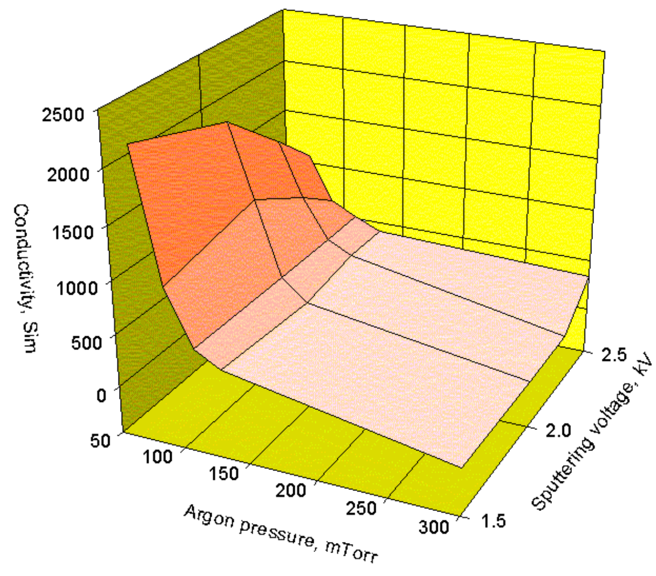

Figure 10. 3-D presentation of tantalum films conductivity as a function of technological factors.